Photocatalytic Oxidation of Sulfur Dioxide in Aqueous Suspension of Fe2O3

ARTICLE *in* THE JOURNAL OF PHYSICAL CHEMISTRY · AUGUST 1989

Impact Factor: 2.78 · DOI: 10.1021/j100354a021

3 AUTHORS, INCLUDING:

Michael R. Hoffmann
California Institute of Technology
417 PUBLICATIONS **30,420** CITATIONS

Photocatalytic Oxidation of Sulfur Dioxide in Aqueous Suspensions of α-Fe_2O_3

Bruce C. Faust,† Michael R. Hoffmann,* and Detlef W. Bahnemann‡

W. M. Keck Laboratories, California Institute of Technology, Pasadena, California 91125
(Received: October 31, 1988; In Final Form: February 3, 1989)

The kinetics and mechanism of the photoassisted autoxidation of S(IV) in aqueous colloidal suspensions of α-Fe_2O_3 have been studied over the pH range of 2–10.5. Similar kinetic behavior toward S(IV) was observed for colloidal suspensions of TiO_2. Quantum yields, ϕ, ranged from 0.08 to 0.3 with a maximum yield found at pH 5.7. Upon band-gap illumination conduction-band electrons and valence-band holes are separated; the trapped electrons are transferred either to surface bound dioxygen or to Fe(III) sites on or near the surface while the trapped holes accept electrons from adsorbed S(IV) to produce S(V). The formation of S(V) radicals indicates that the reaction proceeds via successive one-electron transfers. The relatively high quantum yields are attributed in part to the desorption of $SO_3^{\bullet-}$ from the α-Fe_2O_3 surface and subsequent initiation of a homogeneous free radical chain autoxidation of S(IV) to S(VI). Kinetic and thermodynamic models for the photoassisted surface chemistry of S(IV) on α-Fe_2O_3 are presented.

Introduction

The catalytic autoxidation of SO_2 in deliquescent haze aerosol, clouds, fogs, and hydrometeors appears to be a viable pathway for the rapid formation of sulfuric acid in humid atmospheres.[1-3] Jacob and Hoffmann[4] have shown that Fe(III) and Mn(II) are the most effective catalysts at ambient concentrations for the autoxidations of S(IV) to S(VI) in cloud and fog water. Although Fe(III) has been found in high ($\simeq$1 mM) concentrations in atmospheric water droplets, much of this iron is predicted to be in form of solid particles or colloids on the basis of thermodynamic considerations.[5-12] Ferric oxides and oxyhydroxides (α-Fe_2O_3, Fe_3O_4, α-FeOOH, and γ-FeOOH) have been identified as components of airborne particles;[13] iron-containing particles such as these are likely to serve as cloud and fog condensation nuclei and to be suspended and/or dissolved in the water droplet that results.

Metal oxide semiconductors such as α-Fe_2O_3 (hematite) can function either as photosensitizers or as photocatalysts. Absorption of a photon with an energy equal to or greater than the band-gap energy E_g of a semiconductor results in the transient formation of an electron/hole pair.

$$\alpha\text{-}Fe_2O_3 \xrightarrow{h\nu} e^-_{cb} + h^+_{vb} \qquad (1)$$

In the absence of suitable electron and hole scavengers adsorbed to the surface of a semiconductor particle, recombination occurs within 1 ns. However, when appropriate scavengers are present, the valence-band holes, h^+_{vb} (E^7_H = 2.3 V {oxidation potential}), function as powerful oxidants while the conduction-band electrons, e^-_{cb} (E^7_H = 0.0 V {reduction potential}), function as moderately powerful reductants. Faust,[14] Frank and Bard,[15] and Leland and Bard[16] have shown that S(IV) (e.g., $SO_2{\cdot}H_2O$, HSO_3^-, or SO_3^{2-}) can be readily oxidized on semiconductor surfaces such as α-Fe_2O_3, TiO_2, and CdS and also on iron oxide polymorphs such as α-FeOOH, β-FeOOH, δ-FeOOH, γ-FeOOH, and γ-Fe_2O_3.

Hong et al.[17] have previously studied the photocatalytic oxidation of S(IV) by O_2 in the presence of TiO_2 and a hybrid complex of Co(II) tetrasulfophthalocyanine covalently linked to the surface of TiO_2 particles. Quantum yields in excess of unity (0.5–300) were observed and attributed to the desorption of $SO_3^{\bullet-}$ from the TiO_2 surface and subsequent initiation of a homogeneous free radical chain reaction. In an earlier study, Faust and Hoffmann[18] investigated the photoinduced reductive dissolution of α-Fe_2O_3 by S(IV) under anoxic conditions over the pH range of 2–4. Likewise, the photoreductive dissolution of γ-FeOOH[19,32] and α-FeOOH[20] by various organic compounds has been investigated.

The principal objectives of this paper are to present a detailed study of the kinetics of the heterogeneous photocatalytic oxidation of S(IV) in suspensions of particulate and colloidal α-Fe_2O_3 and to present possible mechanisms that take into account the surface chemistry of hematite.

Experimental Section

Preparation of Fe_2O_3 Colloids. The preparation of optically transparent Fe_2O_3 colloids was based on the observations made initially by Krecke.[21] $FeCl_3{\cdot}3H_2O$ crystals (Baker) were ground with a pestle into a fine powder before preparation of aqueous stock solutions in the concentration range of 5–50 mM $[Fe^{3+}]_{total}$. Immediately following the preparation of the stock solutions, 300 mL of the $FeCl_3$ solution was added dropwise at the rate of 1 drop/s into 1200 mL of boiling water with an initial pH of 7. The solution was subsequently refluxed in a 2-L round-bottom flask. At the end of the reaction, the pH of the solution was found to be within 10% of the value predicted by the following stoichiometry:

$$2FeCl_3 + 3H_2O \rightarrow Fe_2O_3 + 6HCl \qquad (I)$$

* To whom correspondence should be addressed.
† Forestry & Environmental Studies, Duke University, Durham, NC 27706.
‡ Institut für Solarenergieforschung, Sokelantstrasse 5, Hannover, FRG 3000.

(1) Hoffmann, M. R.; Boyce, S. D. *Adv. Environ. Sci. Technol.* **1983**, *12*, 147–189.
(2) Hoffmann, M. R.; Jacob, D. J.; In *SO_2, NO and NO_2 Oxidation Mechanisms: Atmospheric Consideration*; Calvert, J. G., Ed.; Acid Precipitation Series 3; Butterworth: Boston, 1984; pp 101–172.
(3) Penkett, S. A.; Jones, B. M. R.; Brice, K. A.; Eggleton, A. E. J. *Atmos. Environ.* **1979**, *13*, 123–127.
(4) Jacob, D. J.; Hoffmann, M. R. *J. Geophys. Res.* **1983**, *88*, 6611–6621.
(5) Waldman, J. M.; Munger, J. W.; Jacob, D. J.; Hoffmann, M. R. *Tellus* **1985**, *37B*, 91–108.
(6) Munger, J. W.; Jacob, D. J.; Waldman, J. W.; Hoffmann, M. R. *J. Geophys. Res.* **1983**, *88*, 5109–5121.
(7) Jacob, D. J.; Waldman, J. M.; Munger, J. W.; Hoffmann, M. R. *Environ. Sci. Technol.* **1985**, *19*, 730–735.
(8) Waldman, J. M.; Munger, J. W.; Jacob, D. J.; Flagan, R. C.; Morgan, J. J.; Hoffmann, M. R. *Science* **1982**, *218*, 677–680.
(9) Jacob, D. J.; Waldman, J. M.; Munger, J. W.; Hoffmann, M. R. *Tellus* **1984**, *36B*, 272–285.
(10) Jacob, D. J.; Waldman, J. M.; Munger, J. W.; Hoffmann, M. R. *J. Geophys. Res.* **1986**, *91*, 1089–1096.
(11) Jacob, D. J.; Munger, J. W.; Waldman, J. M.; Hoffmann, M. R. *J. Geophys. Rev.* **1986**, *91*, 1073–1088.
(12) Jacob, D. J.; Shair, F. H.; Waldman, J. M.; Munger, J. W.; Hoffmann, M. R. *Atmos. Environ.* **1987**, *21*, 1305–1313.
(13) Fukasawa, T.; Iwatsuki, M.; Kawabuko, S.; Niyazaki, K. *Anal. Chem.* **1980**, *52*, 1784–1787.
(14) Faust, B. C. Ph.D. Thesis, California Institute of Technology, Pasadena, CA, 1985.
(15) Frank, S. N.; Bard, A. J. *J. Phys. Chem.* **1977**, *81*, 1484–1488.
(16) Leland, J. K.; Bard, A. J. *J. Phys. Chem.* **1987**, *91*, 5076–5083.
(17) Hong, A.; Bahnemann, D. W.; Hoffmann, M. R. *J. Phys. Chem.* **1987**, *91*, 6245–6251.
(18) Faust, B. C.; Hoffmann, M. R. *Environ. Sci. Technol.* **1986**, *20*, 943–948.
(19) Waite, T. D.; Morel, F. M. M. *J. Colloid Interface Sci.* **1984**, *102*, 121–137.
(20) Cunningham, K. M.; Goldberg, M. C.; Weiner, E. R. *Photochem. Photobiol.* **1985**, *41*, 409–416.
(21) Krecke, F. W. *Z. Prakt. Chem.* **1871**, *3*, 286–306.

0022-3654/89/2093-6371$01.50/0

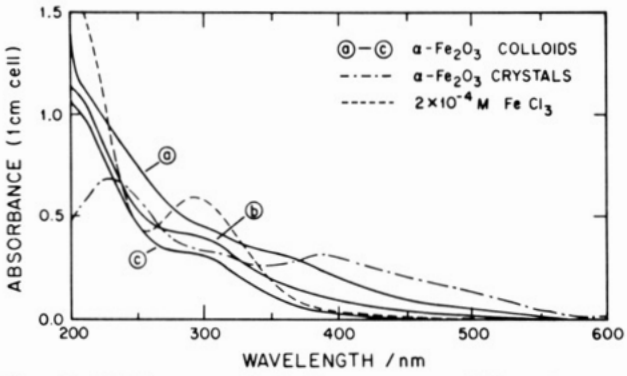

Figure 1. UV/vis spectra of α-Fe_2O_3 transparent colloids and crystals as compared to $FeCl_3$ in aqueous solution at 25 °C. (a) 100 μM colloid immediately after preparation at pH 1.9. (b) 100 μM colloid after solvent evaporation and resuspension in water at pH 2.5. (c) 100 μM colloid followed by titration to pH 1.5, solvent evaporation, and resuspension in water at pH 2.5. For comparison, the UV/vis spectra of α-Fe_2O_3 single crystals calculated for a concentration of 100 μM and an aqueous solution of 200 μM $FeCl_3$ are also shown.

The resulting clear colloidal suspension was dark red in color and exhibited no detectable light-scattering properties. After initial synthesis, 100-mL aliquots of the Fe_2O_3 colloid were dialyzed at 100 °C against water (pH_0 = 5.6) using a Spectropor/2 28.6-mm-diameter dialysis tube (molecular weight cutoff 14000) until the residual Cl^- concentration was reduced to a value $<10^{-5}$ M and the pH of the colloid was $\geq$6.0. The optical absorption spectrum of such a colloidal Fe_2O_3 preparation is shown in Figure 1 along with the spectrum of the unreacted stock solution (diluted to the appropriated concentration) and the spectrum of a thin film of hematite crystals.[22] The onset of absorption of the colloidal preparation starts below 560 nm; this is in excellent agreement with the reported band-gap energy for hematite of 2.2 eV.[22] The transparency of the colloidal solution is evident from the absence of an optical absorption above 600 nm. Although the thin-film spectrum of hematite qualitatively resembles the colloidal spectrum, the absorption coefficient of the single-crystal film is considerably larger in the visible region above 380 nm (cf. Figure 1). Transmission electron microscopy (TEM) reveals that the colloidal preparation was polydisperse in its size distribution with particle diameters distributed between 3 and 25 nm. While it is very likely that bigger particles exhibit the absorption properties of the bulk material, it has recently been shown that the preparation of extremely small particles (e.g., diameters $d \ll 10$ nm) results in so-called Q-size materials with an apparent band-gap shift toward higher energies or lower wavelengths.[23]

The structure of the iron(III) oxide colloids appears to be dependent on the overall synthesis time. When the preparations were refluxed only for the time necessary to complete the addition of the stock solutions, TEM shows particles with an uncharacteristic spherical shape with no apparent crystallinity. Continuous refluxing for at least 24 h did not result in different particle sizes or a different size distribution (see Figure 2). However, a higher degree of crystallinity is apparent from the TEM pictures showing hexagonal and rhombic particles. The electron diffraction pattern confirms the presence of a major fraction of hematite crystals in these preparations, while the smaller particles are likely to be hydrous Fe(III) oxides {e.g., $4Fe_2O_3 \cdot 6H_2O$[24] or $FeOOH \cdot nH_2O$[25]}. As is evident from Figure 2 (bottom), particle sizes, distribution, and shape do not change during dialysis in spite of a substantial shift in pH. Thus our synthesis resulted in clear colloidal suspensions of Fe_2O_3 particles with diameters between

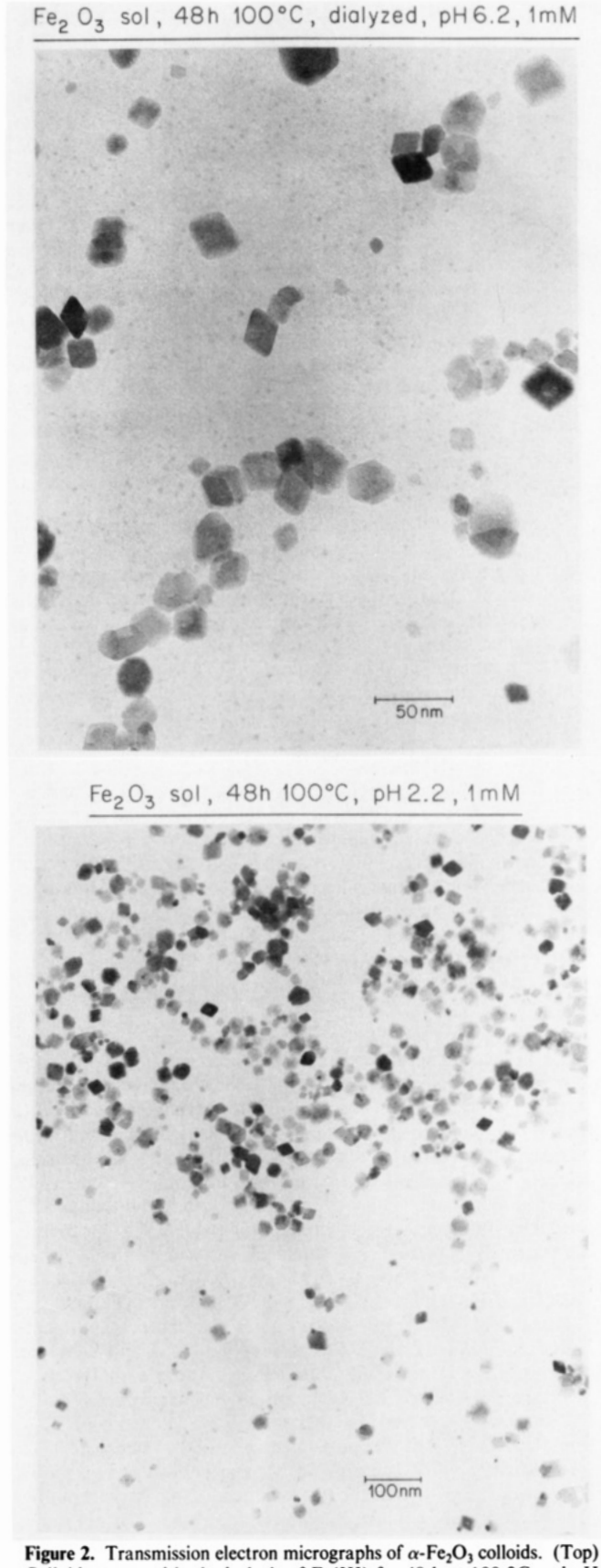

Figure 2. Transmission electron micrographs of α-Fe_2O_3 colloids. (Top) Colloids prepared by hydrolysis of Fe(III) for 48 h at 100 °C and pH 2.5 followed by dialysis to pH 6.2 to yield crystallites with characteristic dimensions in the range of 200–300 Å. (Bottom) Colloids prepared as in the top panel without dialysis.

3 and 25 nm with the majority of the bigger particles possessing the hematite structure. Titration studies revealed that the pH_{zpc} (pH of the zero point of charge where the particle's surface

(22) Marusak, L. A.; Messier, R.; White, W. B. *J. Phys. Chem. Solids* **1980**, *41*, 981–984.
(23) Bahnemann, D. W.; Kormann, C.; Hoffmann, M. R. *J. Phys. Chem.* **1987**, *91*, 3789–3798.
(24) Towe, K. M.; Bradley, W. F. *J. Colloid Interface Sci.* **1967**, *24*, 384–392.
(25) van der Giessen, A. A. *J. Inorg. Nucl. Chem.* **1966**, *28*, 2155.

contains an equal number of positive and negative sites) of these colloidal suspensions was 7.5, which is in the range of reported values for the pH_{zpc}. Fast titration of the dialyzed solutions with base resulted in clear preparations of negatively charged particles above pH 11. All colloids used in this study were stabilized by repulsive electrostatic forces without the addition of colloidal stabilizers.

The preparation of α-Fe_2O_3 colloids with particle sizes greater than 100 nm has been described previously by Faust and Hoffmann.[18] These preparations contained mainly crystalline material with the hematite struture; scanning electron microscopy (SEM) has been used to identify the individual particles as hexagonal platelets with approximate edge dimensions of 0.12 × 0.015 μm. The pH_{zpc} of these particles has been determined to be 8.5.

Titanium dioxide colloids with an average particle diameter of 10 nm were prepared by the controlled hydrolysis of freshly distilled titanium tetraisopropoxide following a procedure described previously.[26]

Reagents and Methods. All reagents were analytical grade. Sodium sulfite (Mallinckrodt) solutions were prepared gravimetrically and standardized with IO_3^-/I^-. Fresh solutions were prepared and stored inside a N_2-atmosphere glovebox (Vacuum Atmospheres Dri-Lab HE-43-2 with HE-493 Dri-Train) for each experiment. The pH of the sulfite solutions was found to decrease only slightly with time $\{\Delta[H^+] = (4 \pm 2) \times 10^{-11}$ M$\}$ for a 0.1 M Na_2SO_3 solution during a 2-week period. The method of Humphrey et al.,[27] which uses DTNB (5,5'-dithiobis(2-nitrobenzoic acid)) as colorimetric reagent, was used for S(IV) determinations in all kinetic experiments. Stock solutions of DTNB were prepared by dissolving the solid in an ethanol/water mixture (95/5 mixing ratio). DTNB reacts quantitatively with SO_3^{2-}, forming 2-nitro-5-sulfhydrobenzoic acid, which has a characteristic absorption spectrum (λ_{max} = 408 nm, $\epsilon_{408\,nm}$ = 15 500 M^{-1} cm^{-1}). During a typical experiment sample aliquots were withdrawn from the photolysis reactor[18] as a function of time, filtered through 0.2-μm filters, and then preserved for S(IV) analysis by derivatization with DTNB. A constant temperature of 25 ± 1 °C was maintained in the reaction vessel with a temperature-controlled recirculating water bath. pH measurements were made with either a Beckman Altex ϕ71 or a Radiometer (Model PHM85) pH meter and a Radiometer combination electrode (GK240B; Ag/AgCl internal reference). Ionic strength was adjusted to 0.1 M with $NaClO_4$ for the large-particle experiments, while the ionic strength in the small-particle experiments was 0.001 M.

Kinetic experiments with the transparent colloids of Fe_2O_3 and TiO_2 were performed at room temperature (22–24 °C) and at atmospheric pressure. Analysis of the ionic reactants and reaction products (e.g., SO_3^{2-}, $S_2O_6^{2-}$, and SO_4^{2-}) was achieved with a Dionex 2000i HPIC equipped with a AS4 separator column and a conductivity detector. The eluent was 2 mM *tert*-butylammonium hydroxide and 1 mM Na_2CO_3 in a water/acetonitrile mixture (90%/10%); the regenerating reagent was 25 mN H_2SO_4.

The procedure of Tamura et al.[28] was employed to measure Fe(II) concentrations using 1,10-phenanthroline with F^- added to complex Fe(III). Total aqueous iron ($[Fe(II)]_{aq} + [Fe(III)]_{aq}$) was determined by reducing soluble Fe(III) to Fe(II) with 0.1 M hydroxylamine sulfate followed by colorimetry with 1,10-phenanthroline. High-purity water (18 MΩ·cm) was obtained from a Millipore Milli-Q system.

The monochromatic illumination system has been described in detail elsewhere.[17,18,23] Actinometry was carried out using Reinecke's salt[29] or Aberchrome 540[30] and was repeated regularly at each wavelength of excitation for quantum yield determinations.

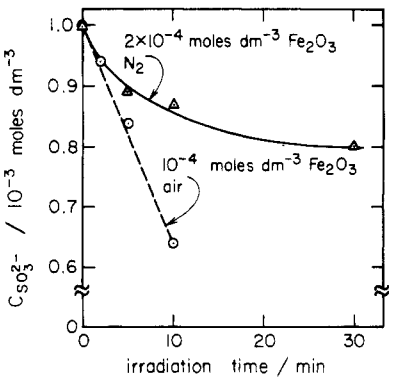

Figure 3. Photooxidation of S(IV) on colloidal α-Fe_2O_3 at pH 3.5 with λ_{ex} = 320 nm in the presence (---) and absence of O_2 (—). In the anoxic case, the reaction ceases upon stoichiometric reductive dissolution of the colloid to give $Fe(II)_{aq}$.

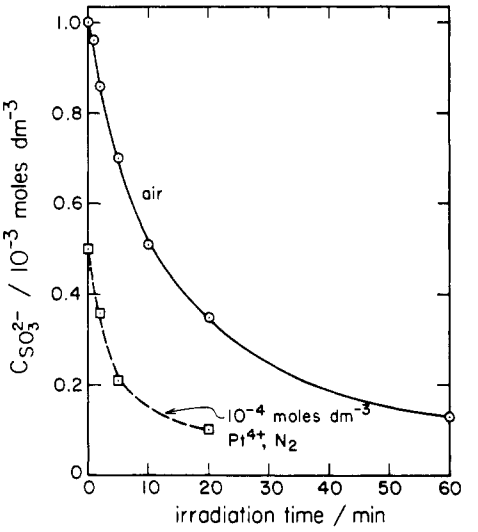

Figure 4. Photooxidation of S(IV) on 10^{-4}/mol/dm^{-3} colloidal α-Fe_2O_3 at pH 6.9 with λ_{ex} = 320 nm in the presence of O_2 (—) and Pt^{4+} as electron acceptors (---).

Spectra were taken with a Shimadzu MPS 2000 spectrophotometer and an associated integrating sphere for turbid samples.

Results

Photooxidation of S(IV) on Small (<30 nm) Fe_2O_3 Particles. S(IV) is readily depleted when colloidal solutions containing 1 mM sulfite and 0.1 mM of the small Fe_2O_3 particles are illuminated (λ_{ex} = 320 nm) in the presence of air at pH 3.5 (dashed line in Figure 3). A quantum yield of 0.095 was determined from the slope of this line taking into account the measured absorptivity of the colloid at 320 nm and the measured photon flux. HPIC analysis indicated that SO_4^{2-} was the only oxidation product formed under these experimental conditions. However, when illumination was carried out in N_2-saturated solutions, both SO_4^{2-} and $S_2O_6^{2-}$ were formed as oxidation products with the concentration ratio being 2.4–2.6 to 1, respectively. As is evident from the solid line in Figure 3, depletion of S(IV) in the anoxic solution has the same initial rate as in the oxic solution but slows down during the course of the experiment until it finally levels off after 0.2 mM SO_3^{2-} was oxidized. This amount was equivalent to the initial concentration of Fe_2O_3 catalyst present in the system. Spectral analysis of the solution used in these anoxic studies showed that the colloid had been dissolved during the irradiations leading to a decrease of optical absorption above 450 nm. Figure 4 shows the comparison of an oxic and an anoxic illumination experiment carried out at pH 6.9. The initial slope of the sulfite depletion at pH 6.9 in an oxic system (solid line in Figure 4) indicated that the quantum yield had increased to ϕ = 0.22. The reaction slows down when the available concentration of the reactants (i.e., S(IV) as HSO_3^- and SO_3^{2-} and O_2) has decreased

(26) Bahnemann, D. W.; Henglein, A.; Lilie, J.; Spanhel, L. *J. Phys. Chem.* **1984**, *88*, 709–711.
(27) Humphrey, R. C.; Ward, M. H.; Hinze, W. *Anal. Chem.* **1970**, *42*, 698–702.
(28) Tamura, H.; Goto, K.; Yotsuyanagi, T.; Nagayama, M. *Talanta* **1974**, *21*, 314–318.
(29) Wegner, E. E.; Adamson, A. W. *J. Am. Chem. Soc.* **1966**, *88*, 394–404.
(30) Heller, H. G.; Langan, J. R. *J. Chem. Soc., Perkin Trans. 2* **1981**, 341.

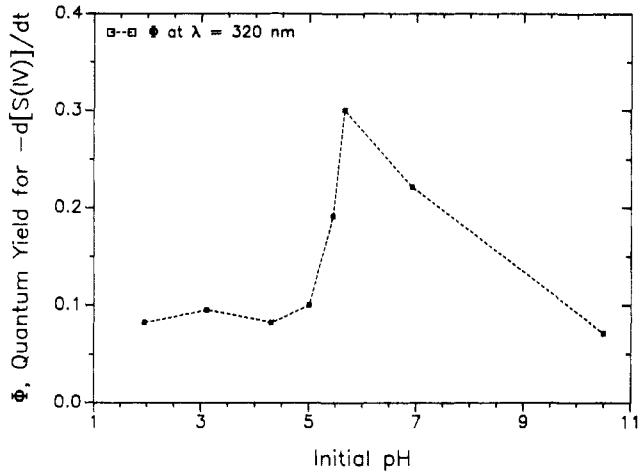

Figure 5. Quantum yield vs pH for the photooxidation of 1.0 mM S(IV) in a colloidal suspension of 0.1 mM Fe_2O_3 in the presence of 0.25 mM O_2.

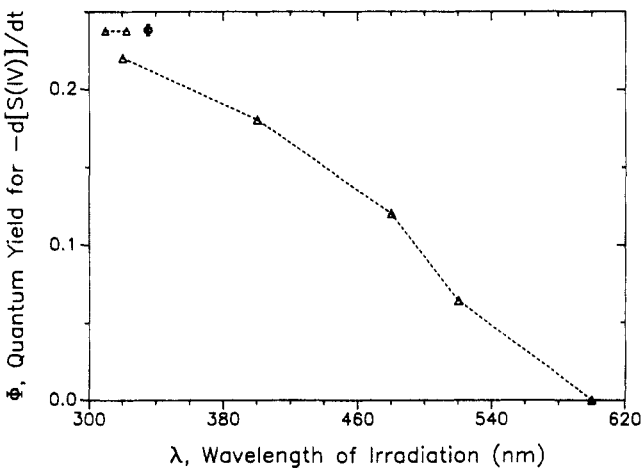

Figure 6. Quantum yield vs wavelength for the photooxidation of 1.0 mM S(IV) in a colloidal suspension of 0.1 mM Fe_2O_3 in the presence of 0.25 mM O_2 at pH 6.9.

and competitive adsorption effects become important. Similar kinetic behavior is observed when 0.1 mM K_2PtCl_6 was substituted for O_2 as an oxidant, thus preventing the dissolution of the photocatalyst as noted in the experiment described in Figure 3 (dashed line in Figure 4). The initial slope of this curve yielded the same quantum yield as the aerated sample. Depletion of the reactants was reponsible for the apparent slowdown of the sulfite oxidation rate at longer illumination times.

Since a marked pH dependence was observed in the experiments described above, the influence of pH on the quantum yield of the S(IV) oxidation over a wider range of conditions was investigated. Figure 5 shows the result of this study (experimental conditions: aerated solutions (0.24 mM O_2) with 1 mM S(IV) and 0.1 mM α-Fe_2O_3 colloid): while the quantum yield shows little variation between pH 2 and 5 (the pH range where HSO_3^- dominates S(IV) speciation), there is a marked increase in the observed rate between pH 5 and 6. A further increase in pH, however, results in a considerable decrease of the S(IV) oxidation rate; this occurs at pH values near and above the pH_{zpc} (7.5) of colloidal Fe_2O_3. Close to the pH_{zpc} the colloidal particles will tend to coagulate while above the pH_{zpc} the surface charge will be dominated by negatively charged surface groups (i.e., □-FeO^-) and thus SO_3^{2-} will have a much smaller tendency to be adsorbed to the surface due to electrostatic repulsion (as will be shown below in a model of the surface speciation).

The wavelength dependence of the quantum yield of the sulfite oxidation measured at pH 6.9 in aerated samples containing 1 mM S(IV) and 0.1 mM Fe_2O_3 colloid is shown in Figure 6. No S(IV) oxidation is observed when illuminations were carried out

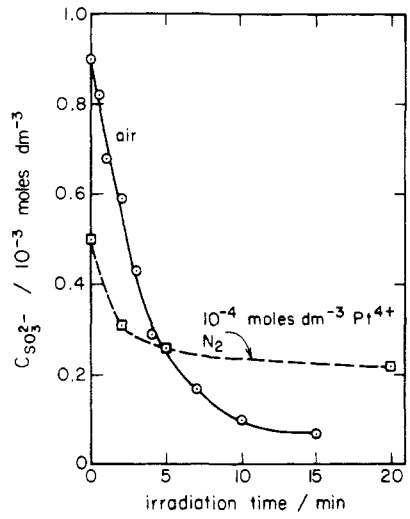

Figure 7. Photooxidation of S(IV) on 3.1×10^{-3} mol dm^{-3} colloidal TiO_2 at pH 2.0 with λ_{ex} = 320 nm in the presence of O_2 (—) and Pt^{4+} as electron acceptors (- - -).

with $\lambda_{ex} > 550$ nm (i.e., with energies below the band-gap energy of hematite). The increase in quantum yield with an increase in excitation energy could be explained by the presence of smaller particles of hydrous Fe_2O_3 or hydrous FeOOH that are excited at shorter wavelengths. Of special interest is that the pH_{zpc} of the colloidal suspension (7.5) is in a range[33] more typical of α-FeOOH and γ-FeOOH than crystalline α-Fe_2O_3 (pH_{zpc} = 8.5). The photoaction spectrum shown in Figure 6 could therefore be understood in terms of an additive effect of oxyhydroxides[31] (e.g., $FeOOH \cdot 1.2H_2O$ and $FeO_{(3-x)/2}(OH)_x$) and crystalline α-Fe_2O_3 present in the samples.

In order to compare the photocatalytic activity of our Fe_2O_3 preparations with that of other established photoactive metal oxides, kinetic studies were also performed using colloidal TiO_2 as a catalyst. Figure 7 shows the oxidation of S(IV) in aqueous solutions containing 3.1 mM TiO_2 at pH 2 both in the absence and in the presence of oxygen. Under oxic conditions a quantum yield of 0.42 was calculated from the initial slope of the S(IV) depletion (solid line in Figure 7), while a ϕ of 0.25 was obtained when Pt^{4+} as $PtCl_6^{2-}$ acts as the electron acceptor in a N_2-saturated sample (dashed line). The shape of the depletion curves shown in this figure are similar to those obtained for the Fe_2O_3 photolyses.

Adsorption of S(IV) on α-Fe_2O_3 in 100-nm Particle Suspensions. Faust and Hoffmann[18] have shown that S(IV) is rapidly adsorbed to the surface of α-Fe_2O_3. The characteristic time for attainment of equilibrium with respect to the formation of surface complexes in the large particle suspensions is on the order of 1 min. An adsorption isotherm for the surface complexation of S(IV) of the following form was found:

$$[S(IV)]_{ads} = \frac{K_1X_1[S(IV)]_{aq}}{1 + K_1[S(IV)]_{aq}} + \frac{K_2X_2[S(IV)]_{aq}}{1 + K_2[S(IV)]_{aq}} \quad (2)$$

where X_1 and X_2 are the molar concentrations of the two distinctly different surface complexes, $[S(IV)]_{aq}$ and $[S(IV)]_{ads}$ are the molar concentrations of all the aqueous and adsorbed S(IV) species, respectively, and K_1 and K_2 are the stability constants for the surface complexes. At pH 2.9 and $[\alpha\text{-}Fe_2O_3]$ = 0.75 mm, $K_1 = 1.1 \times 10^6$ M^{-1}, $X_1 = 1.8 \times 10^{-5}$ M, $K_2 = 2.4 \times 10^3$ M^{-1}, and $X_2 = 4.4 \times 10^{-5}$ M.

Reaction Stoichiometry. The reaction stoichiometry for the autoxidation of S(IV) was determined to be

$$HSO_3^- + 0.5O_2 \xrightarrow[h\nu \geq 300\text{ nm}]{\alpha\text{-}Fe_2O_3} SO_4^{2-} + H^+ \quad (3)$$

The stoichiometry of eq 3 was verified experimentally by deter-

(31) Mulvaney, P.; Swayambunathan, V.; Grieser, F.; Meisel, D. *J. Phys. Chem.* **1988**, *92*, 6732–6740.

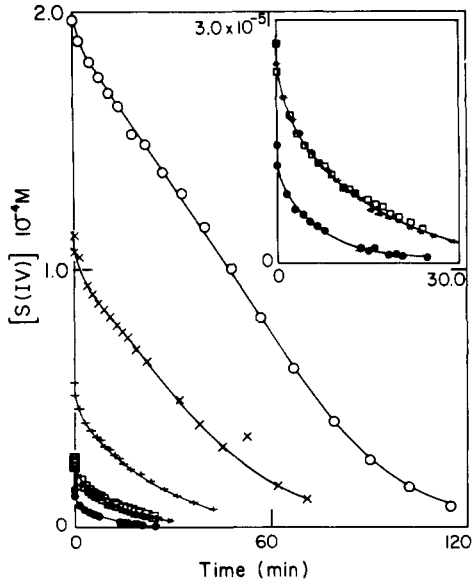

Figure 8. Rate of S(IV) photooxidation as a function of [S(IV)] in suspensions of large-particle hematite ($D_p \simeq 0.15$ μm) with [α-Fe_2O_3] = 82.5 μM, pH 2.4, P_{O_2} = 1.0 atm, and $\lambda \geq 310$ nm. Insert gives an expanded scale for the lower left-hand portion of the graph.

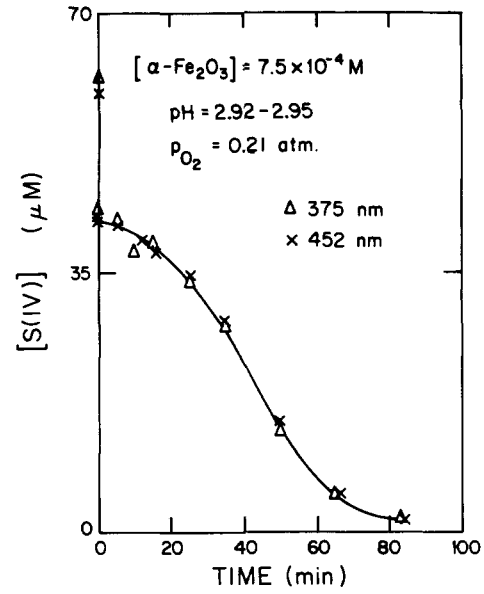

Figure 9. Apparent autocatalytic oxidation of S(IV) at two different wavelengths for large-particle suspensions.

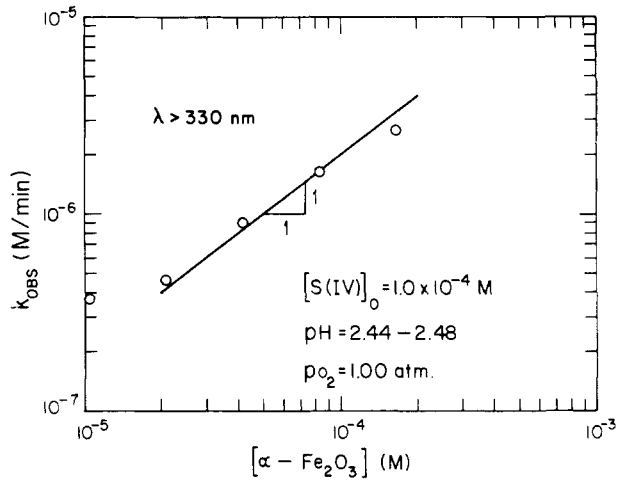

Figure 10. Apparent zero-order rate constant for S(IV) photooxidation as a function of [α-Fe_2O_3] (i.e., as a function of total reactive surface area).

mining the analytical concentrations of S(IV), $O_{2(aq)}$, and SO_4^{2-} both before and after irradiation of an air-saturated aqueous suspension (pH 2.95) of 100-nm hematite particles ([α-Fe_2O_3] = 82.5 μM) with $[S(IV)]_0$ = 0.28 mM and $[O_2]_0$ = 0.24 mM. Results of this experiment gave the following stoichiometric coefficients: $\Delta[O_2]/\Delta[S(IV)] = 0.41$ and $\Delta[S(IV)]/\Delta[S(VI)] = -1.01$. The discrepancy between experimental and theoretical stoichiometric coefficients (0.41 vs 0.5) is mostly likely due to oxygen leakage into the reactor.

Dithionate was observed during the anoxic photooxidation of S(IV) on the small-particle (transparent) suspensions of α-Fe_2O_3 (vide supra) but not during the oxidation in the presence of O_2. Even though α-Fe_2O_3 and O_2 are thermodynamically capable of oxidizing S(IV), O_2 is clearly the principal oxidant in this system. In a control experiment, a deoxygenated solution of S(IV) (0.43 mM) and α-Fe_2O_3 (0.30 mM; 100 nm particles) under N_2 was kept in the dark for 30 min with no detectable production of Fe(II). However, irradiation with visible light (λ = 452 nm) for 3 h produced 12 μM of $Fe(II)_{aq}$. Experiments with oxygenated suspensions containing S(IV) likewise resulted in the release of small but detectable quantities of $Fe(II)_{aq}$. In the dark, the rate of dissolution of a 0.75 mM Fe_2O_3 suspension in the presence of 60 μM S(IV) at pH 2.9 was found to be 0.5 nM min^{-1} (ν = d[Fe(II)]/dt); in the presence of filtered sunlight ($\lambda > 300$ nm), the rate of release of Fe(II) to solution was found to increase to 5.3 nM min^{-1}. Although α-Fe_2O_3 is thermodynamically capable of oxidizing S(IV), the rate of oxidation S(IV) by hematite is substantially slower than by oxygen (Fe(III) catalyzed).

Kinetics of S(IV) Oxidation by O_2 in Large-Particle (>100 nm) Suspensions. As shown in Figure 8, at low [S(IV)] the reaction exhibits an apparent first-order dependence on [S(IV)], while at high [S(IV)] the reaction rate is zero-order with respect to [S(IV)]. Between these concentration extremes the apparent reaction order with respect to [S(IV)] varies between zero and one. This observation is consistent with the concept of saturation kinetics that results from the adsorption of S(IV) on hematite.

At lower light intensities, the rate of S(IV) oxidation increases with time (Figure 9). This apparent autocatalytic behavior suggests either the initiation of a free radical chain sequence or a catalytic sequence involving $Fe(III)_{aq}$ generated by oxidation of $Fe(II)_{aq}$ released during photolysis. The rates of S(IV) autoxidation are nearly identical for λ = 375 and 452 nm (Figure 9). Similar autocatalytic behavior for S(IV) autoxidation was observed at λ = 520 and 600 nm.

To check the possibility of a reaction pathway proceeding via the excitation of a surface-bound S(IV) molecule that was not dependent on the photochemical properties of α-Fe_2O_3, a suspension of alumina, α-Al_2O_3 (structurally identical with α-Fe_2O_3), in the presence of 60 mM S(IV) and 2.5 mM O_2 was irradiated at λ = 375 nm for 2.5 h. During the illumination period no detectable change in [S(IV)] was observed.

The dependence of the observed rate of reaction on the total available surface area is illustrated in Figure 10. The slope of this log–log plot of the pseudo-even-order rate constant, k_{obsd} vs [α-Fe_2O_3] (e.g., [α-Fe_2O_3] $\propto A_s$), is 1, indicating that adsorption to surface active sites is an important pre-equilibrium step in the reaction mechanism.

The overall reaction rate measured in terms of the rate of reduction of O_2 was also found to be autocatalytic as shown in Figure 11. The apparent reaction order with respect to oxygen also exhibited saturation behavior.

Discussion

The Role of Surface Complexation Formation. The photoassisted heterogeneous solution of S(IV) appears to proceed via rapid formation of Fe(III)–S(IV) surface complexes formed by ligand exchange with the surface hydroxyl groups. For example, two possible surface complexes are as follows:

$$\square\text{-FeOH} + HSO_3^- \overset{K_3}{\rightleftharpoons} \square\text{-FeOSO}_2^- + H_2O \qquad (4)$$

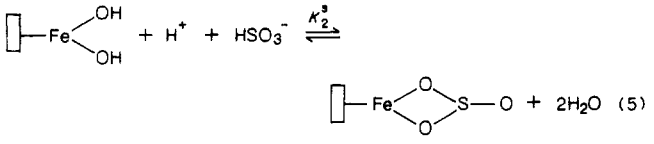

(5)

In the first case, a mononuclear monodentate surface complex is formed, while in the second case a monodentate bidentate complexed is formed. In the pH range of 1–3, the overall rate of reaction is limited by [□-$FeOSO_2^-$] or [□-FeO_2SO] up to the saturation limit imposed by the total number of available surface sites (~10 sites/nm^2). Enhanced reactivity in the pH range of 5–7 can be attributed either to the more favorable surface complexation of SO_3^{2-}, e.g.

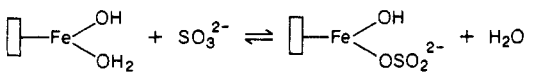

or to the increased contribution of reaction pathways that occur independently of the surface coordination sites. For example, $SO_3^{\bullet-}$ generated at a surface site may diffuse into the bulk phase and initiate a free radical chain reaction involving O_2. Likewise, Fe(II) can be oxidized readily above pH 5 to give Fe(III) which can in turn catalyze the autoxidation of S(IV) in the aqueous phase. Contribution of these pathways to the overall rate of reaction will be discussed below.

The role of surface hydroxyl groups as the principal reactive sites on metal oxide surfaces and as the source of the amphoteric properties of the metal oxides has been clearly established.[32,33] Spectroscopic studies have shown that there are a variety of types of hydroxyl sites present on hydrolyzed metal oxide surfaces.[34-39] Some of the possible surface group configurations are illustrated in Table I. A number of studies have shown that there is a distribution of surface hydroxyl groups (i.e., sites) with a range of acid–base properties.[40-44] A wide variety of ex situ and in situ methods have been employed to establish the nature and structure of surface complexes formed between cations and anions and hydroxylated metal oxide surfaces.[45-54] Hayes et al.[55] have used

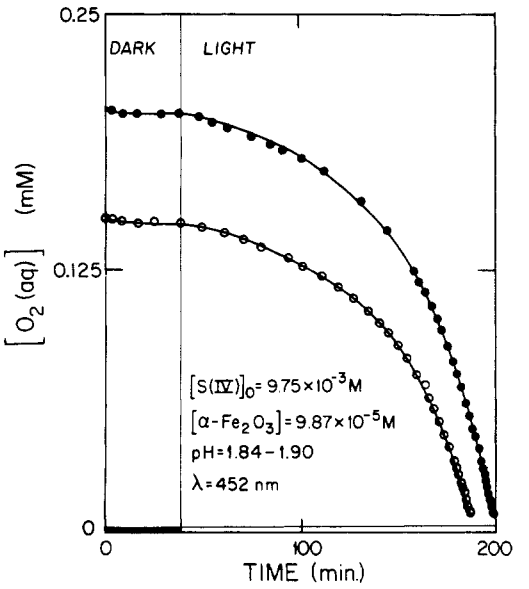

Figure 11. Concentration vs time profiles for the reduction of O_2 during the photooxidation of S(IV) in large-particle suspensions.

TABLE I: Possible Surface Group Configurations for Hydrolyzed Iron(III) Oxide Surfaces[a,b]

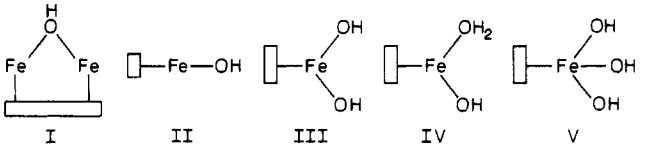

[a] Five different surface hydroxyl groups on α-Al_2O_3 have been identified by Peri;[79] IR spectral differences were attributed to differences in the number of adjacent oxygens. [b] Quantum mechanical calculations suggest that the bridging hydroxyls of I are stronger acids than the terminal groups of II.[80]

EXAFS to show that selenate (SeO_4^{2-}) forms a weakly bound, outer-sphere complex with the surface of α-FeOOH, while selenite (SeO_3^{2-}) forms a strongly bound, inner-sphere complex with the surface of α-FeOOH. The SeO_3^{2-} was found to be bonded directly to the geothite surface in the form of a bidentate complex with two iron atoms 3.38 Å from Se. Their results suggest that HSO_3^- or SO_3^{2-} should form surface complexes on α-Fe_2O_3 analogous to the solution-phase complexes $Fe(OH)SO_3^0$ and $FeOSO_2^+$.[33,56,57]

The principal oxidation product, SO_4^{2-}, can also be expected to form complexes with surface coordination sites, □-$Fe^{III}OH$, similar to solution-phase complexes. Sigg and Stumm[58] have reported intrinsic stability constants for □-$Fe^{III}OSO_3^-$ and □-$(Fe^{III})_2OSO_3$ surface complexes on goethite (α-FeOOH). With a knowledge of the solution stability constants for $FeSO_3^+$ and $FeSO_4^+$, LFER's[33] can be obtained to predict the relative stability of S(IV) vs S(VI) surface complexes with □-$Fe^{III}OH$. The stability constant for the homogeneous complex $FeSO_4^+$ ($Fe^{3+} + SO_4^{2-} \rightleftharpoons FeSO_4^+$) is $10^{2.0}$ M^{-1},[59] while the corresponding stability constant for $FeSO_3^+$ is $10^{6.2}$ M^{-1} at μ = 0.4 M.[57] Therefore, under the conditions of the experiments reported here, S(IV) will be able to displace S(VI) from surface coordination sites, and no inhibition of the photochemical reaction rate by sulfate should be observed.

(32) James, R. O.; Parks, G. A. *Surface Colloid Sci.* **1982**, 119–216.
(33) Schindler, P.; Stumm, W. In *Aquatic Surface Chemistry*; Wiley-Interscience: New York, 1987; pp 83–110.
(34) Rochester, C. H. *Powder Technol.* **1976**, *13*, 157–176.
(35) Rochester, C. H.; Topham, S. A. *J. Chem. Soc., Faraday Trans. 1* **1979**, *75*, 591–602.
(36) Rochester, C. H.; Scurrell, M. S. *Surf. Defect Prop. Solids* **1973**, *2*, 114–139.
(37) Hair, M. L. *Infrared Spectroscopy in Surface Chemistry*; Marcel Dekker: New York, 1967.
(38) Kiselev, A. V.; Lygin, V. I. *Infrared Spectra of Surface Compounds*; Wiley: New York, 1975.
(39) Tsyganenko, A. A.; Felimonov, V. N. *Spectrosc. Lett.* **1972**, *5*, 477–487.
(40) Lavalley, J. C.; Caillod, J. *J. Chim. Phys. Chim. Biol.* **1980**, *77*, 373–377.
(41) Joslin, S. T.; Fowkes, F. M. *Ind. Eng. Chem. Prod. Res. Dev.* **1985**, *24*, 369–375.
(42) Auroux, A.; Vedrine, J. C. *Stud. Surf. Sci. Catal.* **1985**, *20*, 311–318.
(43) Brazdil, J. F.; Yeager, E. B. *J. Phys. Chem.* **1981**, *85*, 1005–1014.
(44) Yamanka, T.; Tanabe, K. *J. Phys. Chem.* **1975**, *79*, 2409–2411.
(45) Bleam, W. F.; McBride, M. B. *J. Colloid Interface Sci.* **1985**, *103*, 124–132.
(46) Parfitt, R. L.; Smart, R. St. C. *J. Chem. Soc., Faraday Trans. 1* **1977**, *73*, 796–802.
(47) Parfitt, R. L.; Russell, J. D.; Farmer, V. C. *J. Chem. Soc., Faraday Trans. 1* **1976**, *73*, 1082–1087.
(48) Rudin, M.; Motschi, H. *J. Colloid Interface Sci.* **1984**, *98*, 385–393.
(49) Tejedor-Tejedor, M. I.; Anderson, M. A. *Langmuir* **1986**, *2*, 203–210.
(50) Burwell, Jr., R. L.; Pearson, R. G.; Haller, G. L.; Tjok, P. B.; Chock, S. P. *Inorg. Chem.* **1965**, *4*, 1123–1128.
(51) Cornet, D.; Burwell, Jr., R. L. *J. Am. Chem. Soc.* **1968**, *90*, 2489–2494.
(52) Kevan, L. *Acc. Chem. Res.* **1987**, *20*, 1–7.
(53) Harvey, D. T.; Linton, R. W. *Colloids Surf.* **1984**, *11*, 81–96.
(54) Anderson, M. A.; Palm-Gerinen, M. H.; Renard, P. N.; Defosse, C.; Rouxhet, P. G. *J. Colloid Interface Sci.* **1984**, *102*, 328–336.
(55) Hayes, K. F.; Roe, A. L.; Brown, G. E., Jr.; Hodgson, K. O.; Leckie, J. O.; Parks, G. A. *Science* **1987**, *238*, 783–786.
(56) Conklin, M. H.; Hoffmann, M. R. *Environ. Sci. Technol.* **1988**, *22*, 883–891.
(57) Conklin, M. H.; Hoffmann, M. R. *Environ. Sci. Technol.* **1988**, *22*, 899–907.
(58) Sigg, L.; Stumm, W. *Colloid Surf.* **1980**, *2*, 101–117.
(59) Smith, R. M.; Martell, A. E. *Critical Stability Constants*; Plenum: New York, 1976.

This prediction is consistent with experimental observations. The LFER comparing □-FeOH vs $FeOH^{2+}$ as coordination centers (log $K_{surface}$ = 0.9 log $K_{solution}$ + 2.4) for the surface complex formation gives a stability constant for reaction 4 of $10^{6.1}$.

The presence of surface hydroxyl groups on α-Fe_2O_3 has been verified by Peck et al.[60] On the basis of the crystal structure of α-Fe_2O_3 the number density of □-FeOH groups can be calculated to be 9/nm^2, while adsorption measurements yield 5–11 groups/nm^2.[14,25,61-63] Even though there are a number of possible surface sites with different energies and acid–base properties, we will assume either that all of the surface hydroxyl groups are identical and are of the same relative energy or that there are two different surface sites of different energies and acid–base properties. The surface hydrolysis reactions for α-Fe_2O_3 can be written as

$$\square\text{-FeOH}_2^+ \overset{K^s_{a1}}{\rightleftharpoons} \square\text{-FeOH} + H^+ \quad (6)$$

$$\square\text{-FeOH} \overset{K^s_{a2}}{\rightleftharpoons} \square\text{-FeO}^- + H^+ \quad (7)$$

where

$$K^s_{a1} = \frac{[\square\text{-FeOH}][H^+]}{[\square\text{-FeOH}_2^+]} \quad (8)$$

$$K^s_{a2} = \frac{[\square\text{-FeO}^-][H^+]}{[\square\text{-FeOH}]} \quad (9)$$

Concentration is expressed in terms of moles per liter, or alternatively for the surface groups concentration can be expressed as moles of surface groups per gram of solid. The acidity constant of eq 8 and 9 are microscopic constants since each loss of a proton reduces the charge on the surface and thus affects the acidity of the neighboring groups. These apparent acidity constants may be written in the form

$$K^s_{ai} = {}^{int}K^s_{ai} e^{F\psi_{H^+}/RT} \quad (10)$$

where ${}^{int}K^s_{ai}$ is the intrinsic acidity constant (i.e., the acidity constant in a hypothetically chargeless environment), ψ_{H^+} is the effective potential difference between the binding site for H^+ and the bulk of the solution, F is the Faraday constant, R is the universal gas constant, and T is the absolute temperature. Likewise, the stability constants for the reactions given in eq 4 and 5 can be written as

$$K^s_1 = {}^{int}K^s_1 e^{F\psi_{HSO_3^-}/RT} = \frac{[\square\text{-FeOSO}_2^-]}{[\square\text{-FeOH}][HSO_3^-]} \quad (11)$$

$$K^s_2 = {}^{int}K^s_2 e^{F\psi_{HSO_3^-}/RT} e^{-F\psi_{H^+}/RT} = \frac{[\square\text{-FeO}_2\text{SO}]}{[\square\text{-Fe(OH)}_2][HSO_3^-][H^+]} \quad (12)$$

where ψ_{H^+} and $\psi_{HSO_3^-}$ are the effective potential differences between the binding sites for the respective species and the bulk solution. The resulting surface charge and potential are the consequence of the charged species in the case of a single monodentate surface complex, □-$FeOSO_2^-$, □-FeO^-, and □-$FeOH_2^+$; the surface charge density can be obtained from titration data[23] by applying a mass balance around the proton (see Table II). The mass balance equation for total iron is given by

$$[\square\text{-FeOH}]_{tot} = [\square\text{-FeOH}] + [\square\text{-FeOH}_2^+] + [\square\text{-FeO}^-] + [\square\text{-FeOFe}^+] + [\square\text{-FeOSO}_2^+] \quad (13)$$

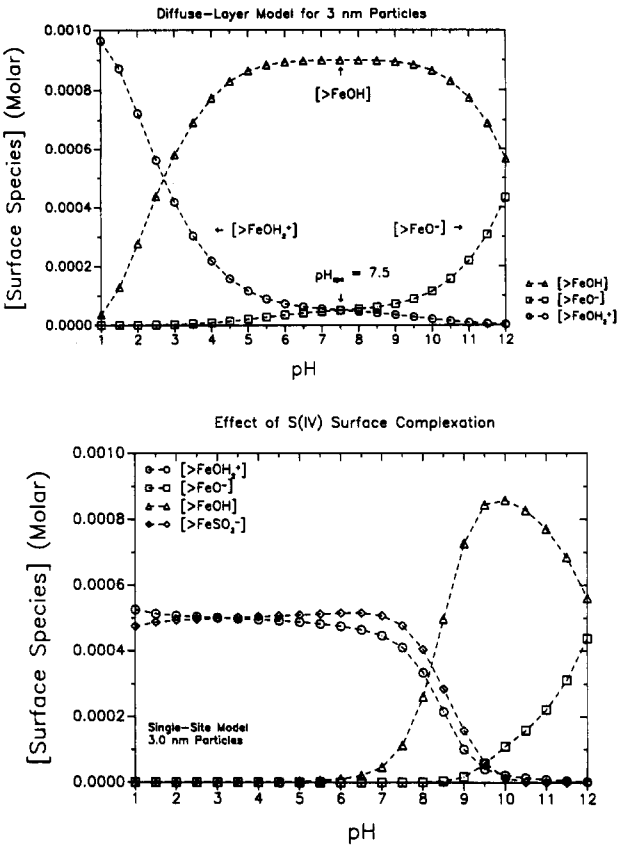

Figure 12. Surface speciation of colloidal hematite particles as a function of pH as computed by SURFEQL according to the approach outlined in Table II. (Top) Speciation of the surface sites vs pH without S(IV). (Bottom) Speciation of the surface sites vs pH with S(IV).

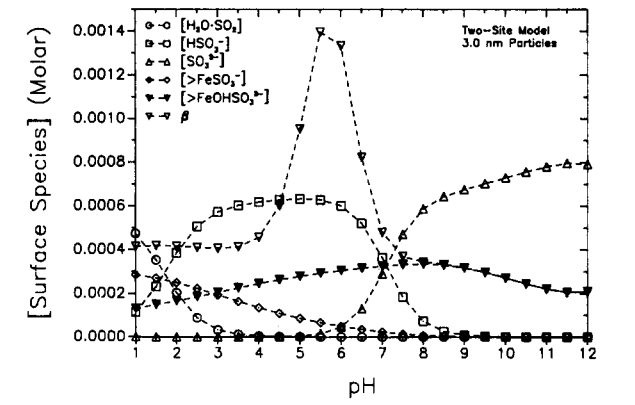

Figure 13. Surface speciation of colloidal hematite particles as a function of pH as computed by SURFEQL according to the approached outlined in Table II and Table III for a two-site complexation model. The function β is given by the sum of the concentrations of the surface complexes and SO_3^{2-} in the electrical double layer at a distance of 3 Å from the particle surface.

where $[\square\text{-FeOH}]_{tot}$ is the total concentration of surface species (see Table II).

Calculation of the surface speciation was made by using the computer code SURFEQL[64,65] in which the diffuse-layer model[66] was used to account for the electrostatic energy associated with the adsorption of metals and ligands on charged surfaces. The diffuse-layer model[66] assumes a layer of fixed charge on the surface of the particles and next to the surface a diffuse layer of opposite

(60) Peck, A. S.; Raby, L. H.; Wadsworth, M. E. *Trans. AIME* **1966**, *235*, 301.
(61) Jurinak, J. J. *Soil Sci. Soc. Am. Proc.* **1966**, *30*, 559.
(62) Breeuwsma, A.; Lyklema, J. *J. Colloid Interface Sci.* **1973**, *43*, 437.
(63) Micale, F. J.; Kiernan, D.; Zettlemoyer, A. C. *J. Colloid Interface Sci.* **1985**, *105*, 570.
(64) Faughnan, J. *SURFEQL—An Interactive Code for the Calculation of Chemical Equilibria in Aqueous Solution*; W. M. Keck Laboratories, California Institute of Technology: Pasadena, CA, 1981.
(65) Morel, F. M.; Morgan, J. J. *Environ. Sci. Technol.* **1972**, *6*, 58.
(66) Westall, J. C.; Hohl, H. *Adv. Colloid Interface Sci.* **1980**, *12*, 265.

TABLE II: Fundamental Features of the Diffuse-Layer Surface Complexation Model[a]

Surface Acidity

$$\square\text{-FeOH}_2^+ \rightleftharpoons \square\text{-FeOH}^0 + H^+_s \qquad K_{a1}^{int}$$

$$\square\text{-FeOH} \rightleftharpoons \square\text{-FeO}^- + H^+_s \qquad K_{a1}^{int}$$

Cation Adsorption

$$\square\text{-FeOH} + Fe^{2+}_s \rightleftharpoons \square\text{-FeOFe}^+ + H^+_s \qquad K_m^{int}$$

Anion Adsorption

$$\square\text{-FeOH} + SO_3^{2-} + H^+_s \rightleftharpoons \square\text{-FeOSO}_2^- + H_2O \qquad K_I^{int}$$

Coulombic Corrections

$$[H_s^+] = [H^+]\exp\left(\frac{-F\Psi_0}{RT}\right)$$

$$[Fe_s^{2+}] = [Fe^{2+}]\exp\left(\frac{-2F\Psi_0}{RT}\right)$$

$$[SO_3^{2-}{}_s] = [SO_3^{2-}]\exp\left(\frac{+2F\Psi_0}{RT}\right)$$

Mole Balance Equations

$$[\square\text{-FeOH}]_{tot} = [\square\text{-FeOH}] + [\square\text{-FeOH}_2^+] + [\square\text{-FeO}^-] + [\square\text{-FeOFe}^+] + [\square\text{-FeOSO}_2^+]$$

$$[Fe(II)]_{tot} = [Fe^{2+}] + [\square\text{-FeOFe}^+] + [FeOH^+] + [FeOH_2]$$

$$[S(IV)]_{tot} = [SO_2{\cdot}H_2O] + [HSO_3^-] + [SO_3^{2-}] + [\square\text{-FeOSO}_2^+]$$

$$[H^+]_{tot} = [H^+] - [OH^-] + \sigma_0 AS/F$$

$$[H^+]_{tot} = [H^+] - [OH^-] + [\square\text{-FeOH}_2^+] + [\square\text{-FeO}^-] - [\square\text{-FeOFe}^+] - [\square\text{-FeOSO}_2^+]$$

$$\sigma = \frac{F}{A_T}[[\square\text{-FeOH}_2^+] + [\square\text{-FeO}^-] - [\square\text{-FeOFe}^+] - [\square\text{-FeOSO}_2^+]]$$

$$\sigma = 0.1174\mu^{1/2}\sinh\left(\frac{zF\Psi_0}{2RT}\right)$$

[a] A = specific surface area (m^2/g), S = solids concentration (g/dm^3), A_T = total surface area [$A_T = AS$] (m^2/dm^3), μ = ionic strength (M), σ = net surface charge (C/m^2), σ_0 = surface proton charge (excess), Φ_0 = potential at surface, tot = total concentration (M), Z = ionic charge, and $\square$ = bulk solid phase. In the case of an uncomplexed surface the surface charge density can be obtained from titration data

$$\sigma = ([\square\text{-FeOH}_2^+] + [\square\text{-FeO}^-])(F/AS) = (C_A - C_B + [OH^-] - [H^+])$$

where C_A and C_B are the resulting concentrations of acid and base, respectively, added during titration of the suspension.

charges distributed in solution according to the Boltzmann distribution. The ψ's in the above equations are replaced by ψ_0's, the surface potentials. Other parameters (e.g., the diffuse-layer capacitance) are given by Gouy–Chapman theory,[66] and thus the electrostatic treatment of the diffuse layer model yields no extraneous fitting parameters aside from ${}^{int}K^s_{a1}$ and ${}^{int}K^s_{a2}$.

The results of a typical calculation of the surface speciation of a suspension of 30-Å particles of Fe_2O_3 in the absence of S(IV) is shown in Figure 12 (top) for the conditions given in Table II. The effect of S(IV) on the surface speciation is shown in Figure 12 (bottom). In the latter case, the S(IV) is found to be strongly bound to a single site on the surface as $\square\text{-FeOSO}_2^-$ over a range of pH from 1 to 7; above pH 7 the surface complex decreases in concentration by a factor of 5 over 2 units of pH. The speciation results are plotted in Figure 13 in terms of the S(IV) distribution for a two-site surface complexation model. The function, β

$$\beta = [\square\text{-FeOSO}_2^-] + [\square\text{-FeOHSO}_3^{2-}] + \alpha[SO_3^{2-}]_{3Å} \qquad (14)$$

shows a pronounced maximum close to the maximum observed

TABLE III: Calculation of the Concentration Profile for S(IV) in the Diffuse Layer[a]

$$[SO_3^{2-}{}_x] = [SO_3^{2-}{}_b]\exp\left(\frac{2e\Psi_x}{kT}\right)$$

$$\frac{d\Psi}{dx} = -\left(\frac{8kTn^\circ}{\epsilon\epsilon_0}\right)^{1/2}\sinh\left(\frac{ze\Psi}{2kT}\right)$$

$$\frac{\tanh(ze\Psi_x/4kT)}{\tanh(ze\Psi_0/4kT)} = e^{-\kappa x}$$

$$\kappa = -\left(\frac{2n^\circ z^2e^2}{\epsilon\epsilon_0 kT}\right)^{1/2} = (3.29\times10^7)zC^{1/2}$$

$$\Psi_0 = \frac{2.3RT}{F}(pH_{zpc} - pH)$$

[a] Φ_0 = the potential at the surface, Φ_x = potential at a distance x away from the surface, C = bulk $z{:}z$ electrolyte concentration in M, κ^{-1} = electrical double layer thickness in cm, n° = bulk ion concentration in number of ions per cm^3, e = charge on the electron, k = Boltzmann constant, z = ionic charge, pH_{zpc} = pH of zero point of charge, ϵ = relative electric permittivity, ϵ_0 = permittivity in a vacuum = 8.854×10^{-14} C V^{-1} cm^{-1}.

in the quantum yield vs pH relationship shon in Figure 5. The function β represents the sum of the concentrations of the surface S(IV) complexes and the calculated concentration of $[SO_3^{2-}]$ at a distance of 3 Å from the particle surface ($[SO_3^{2-}]_{3Å}$ is determined according to the method outlined in Table III where α is a constant). Around the pH_{zpc}, SO_3^{2-} can approach the surface more closely than at higher pH. Thus the net reactions involving either surface complexes or SO_3^{2-} near the surface will be a maximum near the pH_{zpc}.

Mechanism for the Photocatalytic Oxidation of S(IV) on α-Fe_2O_3 Colloids. The experimental results clearly show that small hematite crystals possess photocatalytic activity for the oxidation of S(IV) species. In comparison with similar studies carried out with other photocatalysts such as titanium dioxide,[17] the following mechanism is suggested to account for the experimental observations. Light absorption with photon energies exceeding the band-gap energy of α-Fe_2O_3 (note the wavelength dependence of the observed quantum yield displayed in Figure 6) leads to the formation of electron–hole pairs (eq 1) followed by the one-electron oxidation of adsorbed sulfite yielding the $SO_3^{\cdot-}$ radical anion.

$$\square\text{-FeOSO}_2^- \xrightarrow{h\nu} \underset{e^-_{cb}}{\overset{h^+_{vb} \leftarrow e^-}{\square\text{-FeOS}^{IV}O_2^-}} \rightarrow \underset{e^-_{cb}}{\square\text{-FeOS}^{V}O_2^{\cdot}} \qquad (15)$$

The formation of sulfite radical anion (i.e., $SO_3^{\cdot-}$) intermediates is clearly indicated by the fact that $S_2O_6^{2-}$ is one of the end products when the illuminations are carried out under N_2. It is known from aqueous-phase free-radical chemistry that $SO_3^{\cdot-}$ radicals undergo the following bimolecular recombination and disproportionation reactions in the absence of oxidants such as oxygen.[67]

$$2SO_3^{\cdot-} \rightarrow S_2O_6^{2-} \qquad (16)$$

$$2SO_3^{\cdot-} + H_2O \rightarrow SO_3^{2-} + SO_4^{2-} + 2H^+_{aq} \qquad (17)$$

As predicted by eq 15–17 sulfate and dithionate were detected as the sole oxidation products under anoxic conditions in the relative ratio predicted from the rate constants measured in homogeneous solution.[67] However, under anoxic conditions quantitative dissolution of the hematite particles occurred. Photocorrosion is most likely due to the trapping of the conduction-band electrons formed in reaction 1 at Fe(III) surface sites. In the absence of a suitable electron acceptor bound to the $\square\text{-Fe}^{III}\text{OH}$ surface site (e.g., $\square\text{-Fe}^{III}\text{O=O}$), the $\square\text{-Fe}^{III}\text{OH} + e^-_{cb}$ reaction produces $\square$-Fe(II)OH, which leads to the subsequent release of

(67) Huie, R. E.; Neta, P. *J. Phys. Chem.* **1984**, *88*, 5665–5669.

Fe^{2+}_{aq} to the solution phase and the progressive dissolution of the particle:

$$\underset{e^-_{cb}}{\square\text{-}Fe^{III}OS^{IV}O_2^-\text{-}Fe^{III}OH} \rightarrow \square\text{-}Fe^{III}OS^{V}O_2^{\bullet}\text{-}Fe^{II}OH \quad (18)$$

$$\square\text{-}Fe^{III}OS^{V}O_2^{\bullet}\text{-}Fe^{II}OH \rightleftharpoons Fe^{2+}_{aq} + \square\text{-}Fe^{III}OS^{V}O_2^{\bullet}\text{-}OH \quad (19)$$

Even though the trapping of the conduction-band electron should be rapid, the subsequent dissolution step may be slow. In the following discussion the notation e^-_{tr} will be used to describe a trapped electron (i.e., Fe^{2+} in the α-Fe_2O_3 lattice), while Fe^{2+}_{aq} will refer to solubilized Fe(II). The photocorrosion of Fe_2O_3 via reactions 18 and 19 was reduced dramatically in the presence of alternative oxidants such as Pt^{4+} or Ag^+, which accept e^-_{tr} and thus compete with reaction 18.

$$e^-_{tr} + Pt^{4+}/Ag^+ \rightarrow Pt^{3+}/Ag^0 \quad (20)$$

When O_2 is present in aerated solutions, it could in principle also accept a conduction-band electron to form the superoxide radical O_2^-. However, the redox potential of e^-_{cb} in α-Fe_2O_3 indicates that such an electron transfer should be somewhat improbable since the one-electron redox potential for the $O_2/O_2^{\bullet-}$ couple is –0.33 V (vs NHE),[68] although the redox couple of bound dioxygen may be substantially more favorable as in the case of iron(II) porphyrin–dioxygen complexes and Co(II) Schiff base complexes of dioxygen.[69] In some cases, the $O_2/O_2^{\bullet-}$ potential can be shifted to (+0.82 V).[69] However, in our studies no H_2O_2 has been detected in aqueous suspensions of hematite particles under ultra-band-gap excitation in the presence of a variety of electron donors ($\phi \ll 10^{-4}$).

The stabilizing effect of dioxygen may be the result of an indirect mechanism in which sulfite radical anions formed via reaction 18 react quickly with adsorbed O_2 on the surface of the catalyst particle to form $SO_5^{\bullet-}$ radical anions which in homogeneous solution are known to initate a radical chain reaction that should lead to a very high effective rate of sulfite oxidation under these conditions. Since the quantum yield for the S(IV) depletion is not affected by the absence or presence of O_2 (cf. Figures 3 and 4), we propose that both the $SO_3^{\bullet-}$ and $SO_5^{\bullet-}$ remain bound to surface sites on the small particles (in this case a high fraction of total S(IV) is bound to the surface) where they undergo chemical transformations before products are released into the bulk aqueous phase.

$$\square\text{-}Fe{-}O{-}SO_2^{\bullet} \rightarrow \square\text{-}Fe{-}OSO_4^{\bullet} \quad (21)$$

Several alternative pathways may account for the fate of $SO_5^{\bullet-}$. In one possible pathway, the $SO_5^{\bullet-}$ radical may oxidize the lattice-trapped conduction-band electron forming SO_5^{2-}, thus preventing the dissolution via reaction 19. Peroxomonosulfate, SO_5^{2-}, would then oxidize another molecule of sulfite either on the surface of Fe_2O_3 or in the bulk solution to yield two molecules of sulfate.[71]

$$\underset{e^-_{cb}}{\square\text{-}Fe^{III}OSO_4^{\bullet}} \rightarrow \square\text{-}Fe(III)^+ + SO_5^{2-} \quad (22)$$

$$SO_5^{2-} + HSO_3^- \rightarrow 2SO_4^{2-} + H^+ \quad (23)$$

In another possible pathway, $SO_5^{\bullet-}$ radicals may react with another sulfite molecule on the hematite surface to form $SO_4^{\bullet-}$, which is subsequently reduced to sulfate.[17]

$$\square\text{-}Fe^{III}OSO_4^{\bullet}\text{-}Fe^{III}OSO_3^- + H_2O \rightarrow \square\text{-}Fe^{III}OSO_3^{\bullet}\text{-}Fe^{III}OH + SO_4^{2-} + H^+ \quad (24)$$

$$\underset{e^-_{cb}}{\square\text{-}Fe^{III}OSO_3^{\bullet}\text{-}Fe^{III}OH} + H_2O \rightarrow \square\text{-}Fe^{III}OH\text{-}Fe^{III}OH + SO_4^{2-} + H^+ \quad (25)$$

The observed ϕ vs pH dependence of the quantum yield of S(IV) oxidation on α-Fe_2O_3 (cf. Figure 5) may be due to the influence of several factors. As mentioned above, SO_3^{2-} (pK_{a2} = 7.2) is more readily oxidized in homogeneous solution than HSO_3^-. Similar effects may be operative at the bound surface sites or within the electrical double layer as addressed above and shown in Figures 12 and 13. In a general sense, when pH < pH_{zpc} (i.e., 7.5), the surface charge is dominated by the concentration of $\square$-$FeOH_2^+$ active sites and HSO_3^- and SO_3^{2-} will be preferentially complexed to the surface and accumulated in the electrical double layer near the surface due to electrostatic attraction (i.e., ion-pair formation, outer-sphere complexation) according to the principles of Gouy–Chapman theory. Thus, as the fraction of S(IV) present as SO_3^{2-} increases, provided that the surface remains positively charged, the overall reaction rates are predicted to increase. However, above pH 7 (pH $\simeq$ pH_{zpc}) the net positive charge on the particle surface decreases and the preferential accumulation of SO_3^{2-} in the electrical double layer will decrease; thus the overall rate of reaction as measured by $-d[S(IV)]/dt$ should also decrease. When the pH > pH_{zpc} the particle surfaces have a net negative charge due to the increase in the concentration of $\square$-FeO^- and there will be a net electrostatic repulsion of SO_3^{2-} away from the electrical double layer. However, using basic Gouy–Chapman theory (as shown in Table III), we can calculate the effective concentration of SO_3^{2-} as a function of pH at a distance of 3 Å from the particle surfaces. Provided that electrons can tunnel through a 3–5-Å layer of structured water to the trapped hole on the particle surface, then direct electron transfer ($SO_3^{2-} + h^+_{tr} \rightarrow SO_3^{\bullet-}$) may occur within the electrical double layer. The function, β, shown in the speciation plots of Figure 13 accounts for the accumulation of SO_3^{2-} at a distance of 3 Å from the particle surface. The profile of this function closely approximates the profile of ϕ vs pH shown in Figure 5. A portion of the net reaction that occurs above pH 10 may be due to either the homogeneous free radical chain oxidation of S(IV) or by the Fe(III)-catalyzed autoxidation of S(IV) due to the progressive release of Fe^{2+}_{aq} to solution due to photocorrosion of Fe_2O_3 (vide infra).

We have shown in Figure 7 that S(IV) oxidation proceeds with similar yields and comparable reaction kinetics when colloidal titanium dioxide is used as the photocatalyst instead of small hematite particles. It is interesting to compare the results depicted in Figure 7 with those obtained when larger TiO_2 particles were used as photocatalysts. Hong et al.[17] have shown that quantum yields up to 300 are observed when S(IV) is oxidized in suspensions of Degussa P25 antase particles under ultra-band-gap illumination. A chain reaction mechanism was thus clearly indicated in these suspensions and explained by an initial desorption of the photoproduced $SO_3^{\bullet-}$ radical followed by the well-established free-radical chain in the bulk of the aqueous solution. The role of homogeneous free-radical chains in suspensions of smaller TiO_2 particles (i.e., the diameter of the colloidal particles is at least 5 times smaller than that of the primary particles present in P25 powder) is less clear, since the observed quantum yields were less than one (cf. Figure 7). On the other hand, it has been established in numerous studies that colloidal TiO_2 particles exhibit comparable photocatalytic activities as the Degussa powder[71] and we have no reason to believe the situation should be different in the case of the S(IV) oxidation. Thus the relative ratios of the surface-bound reactants to their bulk-phase counterparts (which will be a function of total reactive surface area) seem to greatly influence the actual mechanism of the photocatalytic process.

In the specific case of photocatalysis on Fe_2O_3, some of the surficial $SO_3^{\bullet-}$ radicals and the $SO_3^{\bullet-}$ radicals generated at a

(68) Bielski, B. H. J.; Cabelli, D. E.; Arudi, R. L.; Ross, A. B. *J. Phys. Chem. Ref. Data* **1985**, *14*, 1041–1100.
(69) Shigehara, K.; Anson, F. C. *J. Phys. Chem.* **1982**, *86*, 2776–2783.
(70) Bahnemann, D. W.; Fischer, Ch.-H.; Janata, E.; Henglein, A. *J. Chem. Soc., Faraday Trans. 1* **1987**, *83*, 2559.
(71) Betterton, E. A.; Hoffmann, M. R. *J. Phys. Chem.* **1988**, *92*, 5962–5965.

distance of 3–5 Å from the surface are able to either react homogeneously within the electrical double layer or diffuse into the bulk solution and react via the following chain mechanism:

$$SO_3^{\bullet-} + O_2 \xrightarrow{k_{26}} SO_5^{\bullet-} \quad (26)$$

$$SO_5^{\bullet-} + HSO_3^- \xrightarrow{k_{27}} SO_4^{\bullet-} + SO_4^{2-} + H^+ \quad (27)$$

$$SO_5^{\bullet-} + SO_3^{2-} \xrightarrow{k_{28}} SO_4^{\bullet-} + SO_4^{2-} \quad (28)$$

$$SO_4^{\bullet-} + HSO_3^- \xrightarrow{k_{29}} SO_3^{\bullet-} + SO_4^{2-} + H^+ \quad (29)$$

$$SO_4^{\bullet-} + SO_3^{2-} \xrightarrow{k_{30}} SO_3^{\bullet-} + SO_4^{2-} \quad (30)$$

$$2SO_3^{\bullet-} \xrightarrow{k_{31}} S_2O_6^{2-} \quad (31)$$

$$2SO_4^{\bullet-} \xrightarrow{k_{32}} S_2O_8^{2-} \quad (32)$$

$$2SO_5^{\bullet-} \xrightarrow{k_{33}} S_2O_8^{2-} + O_2 \quad (33)$$

Hong et al.[17] have mathematically analyzed the reaction system involving the generation of radicals on the surface of TiO_2, diffusion of $SO_3^{\bullet-}$ to the bulk phase, and a free radical chain reaction according to eq 26–33. An additional free radical termination step involves the surficial reaction of $SO_5^{\bullet-}$ as follows:

$$\square\text{-}Fe^{III}OSO_4^{\bullet} + h^+_{vb} \xrightarrow{k_{34}} \square\text{-}Fe^{III}OSO_2^+ + O_2 \quad (34)$$

Given this mechanism the following rate expression has been derived by Hong et al.[17] in the case of photocatalysis by large particle suspensions of TiO_2 for pH < 5:

$$-\frac{d[S(IV)]}{dt} = -\frac{k_{27}k_{34}}{4k_{33}}\{M_xO_y\}[HSO_3^-] + [HSO_3^-]\left\{\left[\frac{k_{27}k_{34}}{4k_{33}}\right]^2\{M_xO_y\}^2 + \frac{k_{27}^2}{2k_{33}}\phi I_0(1 - 10^{-\epsilon L\{M_xO_y\}})\left[\frac{K[HSO_3^-]}{1 + K[HSO_3^-]}\right]\right\}^{1/2} \quad (35)$$

In the case of large-particle suspensions of TiO_2,[17] ϕ ranged from 0.5 to 300. Quantum yields in excess of 1 provide strong evidence for a free radical chain mechanism. In the present study, the quantum yields for the ultrasmall Fe_2O_3 and TiO_2 particles ranged from 0.09 to 0.40. These quantum yields are relative high compared to other photoassisted semiconductor-catalyzed redox reactions; thus some contribution to the overall rate may in fact be due to a homogeneous free radical chain pathway with a very low concentration of freely diffusing initiator radicals (i.e., $SO_3^{\bullet-}$, $SO_4^{\bullet-}$, $^{\bullet}OH$).

A homogeneous free radical pathway in the photocatalytic autoxidation of S(IV) in the presence of Fe_2O_3 may have multiple initiation steps. They include (i) generation of $SO_3^{\bullet-}$ on the surface or within the electrical double layer and (ii) generation of $SO_3^{\bullet-}$ in the homogeneous phase via reactions (e.g., $Fe(bipy)_3^{3+} + SO_3^{2-} \rightarrow Fe(bipy)_3^{2+} + SO_3^{\bullet-}$; $k = 2.1 \times 10^8$ M^{-1} s^{-1})[72] or due to initiation by $^{\bullet}OH$ radical[70,73-77] which has diffused away from the surface. These pathways proceed in parallel to the nonradical pathway catalyzed by Fe(III). In the small-particle studies, the ratio of $[S(IV)]_{aq}/[\square\text{-}FeOSO_2^-]$ was calculated to be close to 1 over a broad range of pH (i.e., 2–8), while in the large-particle studies, this ratio ranged from 10 to 10^2. In photolyses involving the colloidal suspensions, most of the S(IV) chemistry had likely taken place on or near the surface since most of the S(IV) was associated with the surface or accumulated in the double layer. In photolysis with the larger particle suspensions, a significant fraction of S(IV) autoxidation was likely to have taken place in the bulk phase.

An alternative surface mechanism involving electron transfer to bound dioxygen can not be totally excluded at this point in time. This mechanism involves the preequilibrium coadsorption of both S(IV) and O_2 at $\square$-FeOH surface sites followed by band-gap excitation that leads to the transfer of electrons from adsorbed S(IV) to h^+_{vb} and the transfer of electrons from the conduction band to adsorbed O_2.

$$\square\text{-}FeOH + HSO_3^- \overset{K_1^s}{\rightleftharpoons} \square\text{-}FeOSO_2^- + H_2O \quad (36)$$

$$\square\begin{matrix}\text{-}FeOH_2^+ \\ \text{-}FeOSO_2^-\end{matrix} + O_2 \overset{K_3^s}{\rightleftharpoons} \square\begin{matrix}\text{-}FeO{=}O^+ \\ \text{-}FeOSO_2^-\end{matrix} + H_2O \quad (37)$$

$$\square\begin{matrix}\text{-}FeO{=}O^+ \\ \text{-}FeOSO_2^-\end{matrix} \xrightarrow{h\nu} \square\begin{matrix}\text{-}FeO{=}O^+ \\ \text{-}FeOSO_2^- \\ h^+_{vb}\end{matrix} \xrightarrow{k_{38}} \square\begin{matrix}\text{-}FeO{-}O^{\bullet} \\ \text{-}FeOS^{V}O_2^{\bullet}\end{matrix} \quad (38)$$

$$\square\begin{matrix}\text{-}FeO{-}O^{\bullet} \\ \text{-}FeOSO_2^{\bullet}\end{matrix} \xrightarrow{k_{39}} \square\begin{matrix}\text{-}FeO{-}O^- \\ \text{-}FeOSO_2^+\end{matrix} \quad (39)$$

$$\square\begin{matrix}\text{-}FeO{=}O^- \\ \text{-}FeOSO_2^+\end{matrix} + 2H_2O \overset{K_{des}}{\rightleftharpoons} \square\begin{matrix}\text{-}FeOH \\ \text{-}FeOH\end{matrix} + SO_3 + H_2O_2 \quad (40)$$

$$SO_3 + H_2O \xrightarrow{fast} 2H^+ + SO_4^{2-} \quad (41)$$

$$HSO_3^- + H_2O_2 \xrightarrow{fast} H^+ + SO_4^{2-} + H_2O \quad (42)$$

If we assume that the reaction of bisulfite with the surface is the dominant reaction over the pH range of 2–5 and that the adsorption process can be described in terms of a competitive single-site adsorption isotherm, then the rate expression that arises from this surface-limited band-gap excitation mechanism is

$$\nu = \phi I_0(1 - 10^{\epsilon[Fe_2O_3]L})\left(\frac{K_1^sK_3^s[HSO_3^-]_{aq}[O_2]_{aq}}{(1 + K_1^s[HSO_3^-]_{aq} + K_3^s[O_2]_{aq})^2}\right) \quad (43)$$

where ϕ is the intrinsic quantum yield {i.e., $S(IV) + h^+_{vb} \rightarrow SO_3^{\bullet-}$}, K_1^s and K_3^s are the surface binding constants (i.e., the adsorption equilibrium constants), I_0 is the incident photon flux (einstein min^{-1}), $\{Fe_2O_3\}$ is the concentration of photocatalyst (M), and ϵ is the molar absorptivity of the solid (M^{-1} cm^{-1}).

If O_2 adsorption is relatively constant over the pH range of interest and P_{O_2} is held constant, then eq 43 can be reduced to the following form (i.e., first-order kinetics with respect to [S(IV)]; cf. Figure 8):

$$\nu = \alpha\phi I_0(1 - 10^{\epsilon[Fe_2O_3]L})\left(\frac{K_1^s[HSO_3^-]_{aq}}{(1 + K_1^s[HSO_3^-]_{aq})}\right) \quad (44)$$

where α is a constant. When the surface sites are saturated (e.g., $K_1^s[HSO_3^-]_{aq} \gg 1$), the rate expression reduces to the simple form (i.e., zero-order kinetics; cf Figure 8):

$$\nu = \alpha\phi I_0(1 - 10^{\epsilon[Fe_2O_3]L}) \quad (45)$$

However, it is possible that when the reactive surface sites are preferentially bound with S(IV), conduction-band electrons will be shunted to Fe(III) sites in the lattice to produce Fe(II) which is eventually released to solution. The limiting case for the latter process is shown clearly in Figure 3, when O_2 is absent altogether.

Faust[14] has proposed three general steps for the autocatalytic oxidation of S(IV) due to the photoinduced production of $Fe(II)_{aq}$; they include (i) production of $Fe(II)_{aq}$ from photoinduced electron transfer from surficial S(IV) to Fe(III) in the lattice,[18] (ii) induced

(72) Matthews, R. W. *J. Chem. Soc., Faraday Trans. 1* **1984**, *80*, 457–471.
(73) Matthews, R. W. *Water Res.* **1986**, *20*, 569–578.
(74) Cunningham, K. M.; Goldberg, M. C.; Weiner, E. R. *Environ. Sci. Technol.* **1988**, *22*, 1090–1097.
(75) Jaeger, C. D.; Bard, A. J. *J. Phys. Chem.* **1979**, *83*, 3146–3152.
(76) Fujihara, M.; Satoh, Y.; Osa, J. *J. Electroanal. Chem. Interfacial Electrochem.* **1981**, *126*, 277–281.
(77) Mulvaney, P.; Cooper, R.; Grieser, F.; Meisel, D. *Langmuir* **1988** *4*, 1206–1211.

oxidation of $Fe(II)_{aq}$ by $SO_5^{\bullet-}$ or SO_5^{2-} and S(IV) by O_2, and (iii) the $Fe(III)_{aq}$-catalyzed autoxidation of S(IV).[57]

Leland and Bard[16] found that the rate of photooxidation of sulfite in the presence of iron oxide polymorphs varied by 2 orders of magnitude with the relative order of γ-FeOOH > α-Fe_2O_3 > γ-Fe_2O_3 > δ-FeOOH > β-FeOOH > α-FeOOH. They attributed this relative order in the S(IV) oxidation rate to differences in the crystal and surface structure as opposed to differences in reactive surface area, hydrodynamic surface diameter, or band gap. In oxygenated system they found no Fe^{2+} released to solution after photolysis of S(IV) at pH 4.1. Meisel and co-workers[31,78] have recently studied the dynamics of charge transfer from reduced methylviologen radicals to Fe(III) oxides and oxyhydroxide colloids in aqueous suspensions. They found that a fraction of the electrons transferred to the α-Fe_2O_3 colloids were able to migrate into the particle interior and form stable Fe_3O_4. The remaining fraction of transferred electrons formed Fe(II) which was either released to the bulk solution or adsorbed to the particle surface; as the particle size and pH decreased, the fraction of electrons trapped at the surface increased. In addition, they[31] found that the rate of electron transfer from the reduced methylviologen radical is governed by the free energy difference between the redox potential of the redox couple in the electrolyte and the Fermi level in the solid and by the electrostatic interaction between the reduced radical and the electrical double layer. The electrostatic effects between the charged electron donor and the particle surface were found to be the dominant factor contributing to the observed rate constant. Somewhat similar results had been noted previously by Stramel and Thomas.[78]

Acknowledgment. We gratefully acknowledge the financial support of the U.S. Environmental Protection Agency (R8116112-01-0 and R8113326-01-0). We are also grateful for the assistance provided by Drs. Liyuan Liang and Claudius Kormann.

Registry No. Fe_2O_3, 1309-37-1; SO_3^{2-}, 14265-45-3; SO_4^{2-}, 14808-79-8; $S_2O_6^{2-}$, 14781-81-8; O_2, 7782-44-7; Pt^{4+}, 22541-31-7.

(78) Stramel, R. D.; Thomas, J. K. *J. Colloid Interface Sci.* **1986**, *110*, 121-129.

(79) Peri, J. B. *J. Phys. Chem.* **1965**, *69*, 220-230.

(80) Kawakami, H.; Yoshida, S. *J. Chem. Soc., Faraday Trans. 2* **1985**, *81*, 1117-1127.

Formation and Stability of Intramolecular Three-Electron S.∴N, S.∴S, and S.∴O Bonds in One-Electron-Oxidized Simple Methionine Peptides. Pulse Radiolysis Study

K. Bobrowski*

Department of Biophysics, Institute of Biochemistry and Biophysics, Polish Academy of Sciences, Rakowiecka 36, 02-532 Warsaw, Poland

and J. Holcman*

Accelerator Department, Risø National Laboratory, DK 4000 Roskilde, Denmark
(Received: November 16, 1988)

Intramolecular sulfur-sulfur $(S.\therefore S)^+$ and sulfur-nitrogen $(S.\therefore N)^+$ three-electron-bonded radical cations and sulfur-oxygen (S.∴O) radicals have been generated in aqueous solutions of some simple di-, tri-, and tetrapeptides containing methionine units due to oxidation by hydroxyl radicals under pulse radiolysis conditions. All these transient species are formed at the diffusion-controlled rate ($k \geq 10^{10}$ dm^3 mol^{-1} s^{-1}), and they exhibit optical absorptions with the maxima at 390 nm (S.∴N- and S.∴O-bonded species) and at 490 nm (S.∴S-bonded species) with extinction coefficients of 5000-7000 dm^3 mol^{-1} cm^{-1}. In slightly acidic solutions of tri- and tetrapeptides, a protolytic equilibrium between S.∴O- and S.∴S-bonded species was observed. The position of this equilibrium shifts by approximately 2 pK units when going from L-Met-Gly-L-Met (pK = 3.05) to L-Met-Gly-L-Met-L-Met (pK = 5.15). Conversion of the S.∴O-bonded species into the S.∴S-bonded species proceeds via kinetically distinct $[H^+]$-dependent ($k = 10^7$-10^8 dm^3 mol^{-1} s^{-1}) and $[H^+]$-independent ($k \cong 10^4$ s^{-1}) routes. In the pH range 6.0-9.0, a pH- and buffer-concentration-independent conversion of the 490-nm into the 390-nm absorption band was observed. This fast process ($k > 10^5$ s^{-1}) is consistent with the conversion of the S.∴S-bonded species into the S.∴N-bonded species.

Introduction

In the past few years, a growing interest in oxidation processes in biological systems has stimulated several investigations of the radiolysis of sulfur-containing amino acids.[1-4] It has been shown[5] in the dimeric mixed-valence complex $[(Ru(NH_3)_5)_2$-(1.5DTCO)$]^{5+}$ that two neighboring thioether groups facilitate electron transfer in a way that is similar to that in compounds where the thioether group is adjacent to another lone-pair donor such as carboxyl or hydroxyl.[6] Moreover, interaction of the oxidized sulfur center with the latter groups can result in a lowering of the reduction potential which, in the case of 2,6-*endo*,*endo*- and 2,6-*exo*,*endo*-thiomethyl carboxylate derivatives of norbornane, was confirmed by Glass et al.[6]

Similar effects are expected to occur in proteins. They might well evolve from more efficient charge stabilization due to conformational changes leading to favorable mutual positioning of the electron donor-acceptor pairs. A conformational change resulting in a substantial decrease in the reduction potential of

(1) Packer, E. J. *J. Chem. Soc., Perkin Trans. 2* **1984**, 1015.
(2) Buchanan, J. D.; Armstrong, D. A. *Int. J. Radiat. Biol.* **1976**, *30*, 115.
(3) Hiller, K.-O.; Masloch, B.; Göbl, M.; Asmus, K.-D. *J. Am. Chem. Soc.* **1981**, *103*, 2734.
(4) Davies, M. J.; Gilbert, B. C.; Norman, R. O. C. *J. Chem. Soc., Perkin Trans. 2* **1983**, 731.
(5) Stein, C. A.; Taube, H. *J. Am. Chem. Soc.* **1978**, *100*, 1635.
(6) Glass, R. S.; Duchek, J. R.; Klug, J. T.; Wilson, G. S. *J. Am. Chem. Soc.* **1977**, *99*, 7439.

0022-3654/89/2093-6381$01.50/0